


Article

Removal of Specular Reflection Using Angle Adjustment of Linear Polarized Filter in Medical Imaging Diagnosis

Kicheol Yoon ^{1,2,†}, Jaehwang Seol ^{3,4,†} and Kwang Gi Kim ^{1,2,3,4,*} 

- ¹ Medical Devices R&D Center, Gachon University Gil Medical Center, 21, 774 Beon-gil, Namdong-daero, Namdong-gu, Incheon 21565, Korea; kcyoon98@gachon.ac.kr
- ² Department of Biomedical Engineering, College of Medicine, Gachon University, 38-13, 3 Beon-gil, Dokjom-ro 3, Namdong-gu, Incheon 21565, Korea
- ³ Department of Biomedical Engineering, College of Health Science, Gachon University, 191 Hambak-moero, Yeonsu-gu, Incheon 21936, Korea; tjfwoghkd@gachon.ac.kr
- ⁴ Department of Health Sciences and Technology, Gachon Advanced Institute for Health Sciences and Technology (GAIHST), Gachon University, 38-13, 3 Beon-gil, Dokjom-ro, Namdong-gu, Incheon 21565, Korea
- * Correspondence: kimkg@gachon.ac.kr; Tel.: +82-32-458-2880
- † Kicheol Yoon and Jaehwang Seol equally contributed to the work. Kicheol Yoon and Jaehwang Seol are the co-first (lead) authors.

Abstract: The biggest problem in imaging medicine is the occurrence of light reflection in the imaging process for lesion diagnosis. The formation of light reflection obscures the diagnostic field of the lesion and interferes with the correct diagnosis of the observer. The existing method has the inconvenience of performing a diagnosis in a state in which light reflection is suppressed by adjusting the direction angle of the camera. This paper proposes a method for rotating a linear polarization filter to remove light reflection in a diagnostic imaging camera. Vertical polarization and horizontal polarization are controlled through the rotation of the filter, and the polarization is adjusted to horizontal polarization. The rotation angle of the filter for horizontal polarization control will be 90°, and the vertical and horizontal polarization waves induce a 90° difference from each other. In this study, light reflection can be effectively removed during the imaging process, and light reflection removal can secure the field of view of the lesion. The removal of light reflection can help the observer's accurate diagnosis, and these results are expected to be highly reliable and commercialized for direct application in the field of diagnostic medicine.

Keywords: diagnosis; camera imaging; specular reflection removal; linear polarized filter; Malus' law



Citation: Yoon, K.; Seol, J.; Kim, K.G. Removal of Specular Reflection Using Angle Adjustment of Linear Polarized Filter in Medical Imaging Diagnosis. *Diagnostics* **2022**, *12*, 863. <https://doi.org/10.3390/diagnostics12040863>

Academic Editors: Cecilia Di Ruberto, Andrea Loddo, Lorenzo Putzu, Alessandro Stefano and Albert Comelli

Received: 9 March 2022

Accepted: 28 March 2022

Published: 30 March 2022

Publisher's Note: MDPI stays neutral with regard to jurisdictional claims in published maps and institutional affiliations.



Copyright: © 2022 by the authors. Licensee MDPI, Basel, Switzerland. This article is an open access article distributed under the terms and conditions of the Creative Commons Attribution (CC BY) license (<https://creativecommons.org/licenses/by/4.0/>).

1. Introduction

Modern medicine requires diagnostic imaging and preventive medicine. Most imaging medicine uses X-ray, MRI, CT, ultrasound, microscope, and cameras for precise diagnosis [1]. The precision diagnosis camera enables the real-time observation of lesions [2–5]. The diagnostic camera adjusts the brightness of the LED to allow imaging in dark tissue [6]. The disadvantage of the camera during the imaging process is the reflected light (specular reflection) from the lesion due to the light of the LED irradiated to the lesion. The light reflection generated by the LED interferes with the observation field of the lesion. In addition, the generation of light reflections prevents accurate diagnosis. Therefore, the emergence of light reflection makes it very difficult to observe the lesion [7].

For tissue diagnosis, if light reflection is created due to the strong light intensity of the LED, the diagnostic field of view is blocked during the monitoring process of the camera. For example, when light reflection generates on the lesion for observation, the lesion cannot be seen, making it difficult to make an accurate diagnosis.

In order to suppress the occurrence of light reflection in the medical diagnosis field, there is a cumbersome need to change the orientation angle of the camera. In addition,

the observer faces the cumbersome and complicated process of compensating for light reflection using separate software when shooting is completed. In these methods, it is difficult to expect a rapid diagnosis, and the color of the lesion may be lost in the course of the observer's work. Then, the patient and the doctor in charge of diagnosis cannot expect accurate diagnosis results. To overcome this problem, several methods for light reflection suppression have been studied [8]. However, research cases are still lacking, and the traditional trick method used in the field of medical diagnosis has been investigated. Most of the medical field has used a method of minimizing light reflection by adjusting the camera's direction angle [9].

To obtain the polarization effect of the camera, there is a method of irradiating the focal point of the LED in various directions and a method of controlling the beam focal length of the LED [10]. However, it is not easy in the field to adjust the beam irradiation direction angle and focal length of the LED during the diagnosis process [11]. In addition, the best imaging condition for light reflection suppression is to detect specular reflections generated in the spatial conversion process with RGB color functions for the brightness and color of the camera [12]. The detected specular reflection removes the reflection region through deconvolution analysis in the wavelength band. The color image lost due to specular reflection removal restores the lost color through the use of a separate function [12]. This reflected wave cancellation process requires a lot of data and calculation work, which requires complex mathematical operations [12]. The method of collecting frames through continuous shooting requires that the reference image be trained in advance [13]. In this method, the sum and difference are calculated by comparing the interval between the actual shooting frames and the reference training image interval. Then, the reflected light is removed by removing the image of the difference value [13]. However, various cumbersome data collection processes for learning the reference image, lesion data, and normal tissue data follow [14].

There is a method that involves using a polarizing filter in the camera and a method using a sensor that detects only the RGB values of the image by automatically detecting changes in the image [15–18]. However, the method of applying the polarizing filter reduces the shooting radius due to material loss of the filter and provides a dark image. Moreover, the RGB value detection method does not take into account the expected image loss and distortion due to material loss in the filter [15–18].

Research is needed to overcome the complex process of data collection and mathematical operation to suppress the light reflection of photographed data. This study is judged to be usefully applied to the field of medical diagnosis. This paper proposes a method for removing light reflection of an imaging camera. In order to remove light reflection, the filter controls vertical and horizontal polarizations through rotation with 90° , which induces the 90° difference from each other. At this time, the filter used is the linear polarized filter. Section 1 introduces the motivation for this study. Sections 2 and 3 present the research methods and results, and Section 4 a discussion. Lastly, Section 5 concludes the article.

2. Analysis for Removal of Specular Reflection

In the diagnostic endoscopy procedure, a camera is inserted into the organ as shown in Figure 1, and the endoscope camera confirms the lesion status of the mucosa. When photographing a dark organ from a picture, the camera surroundings irradiate the LED on the tissue to capture a bright image.

The large problem in the endoscopic camera imaging process is the emergence of light reflection, as shown in Figure 2 [7]. The occurrence of light reflection obstructs the observation field of the lesion, making it difficult for an observer to make an accurate diagnosis. This light reflection controls the polarization direction of the filter by analyzing the characteristics of polarization and Malus' law [19–21]. In consequence, the light reflection can be eliminated.

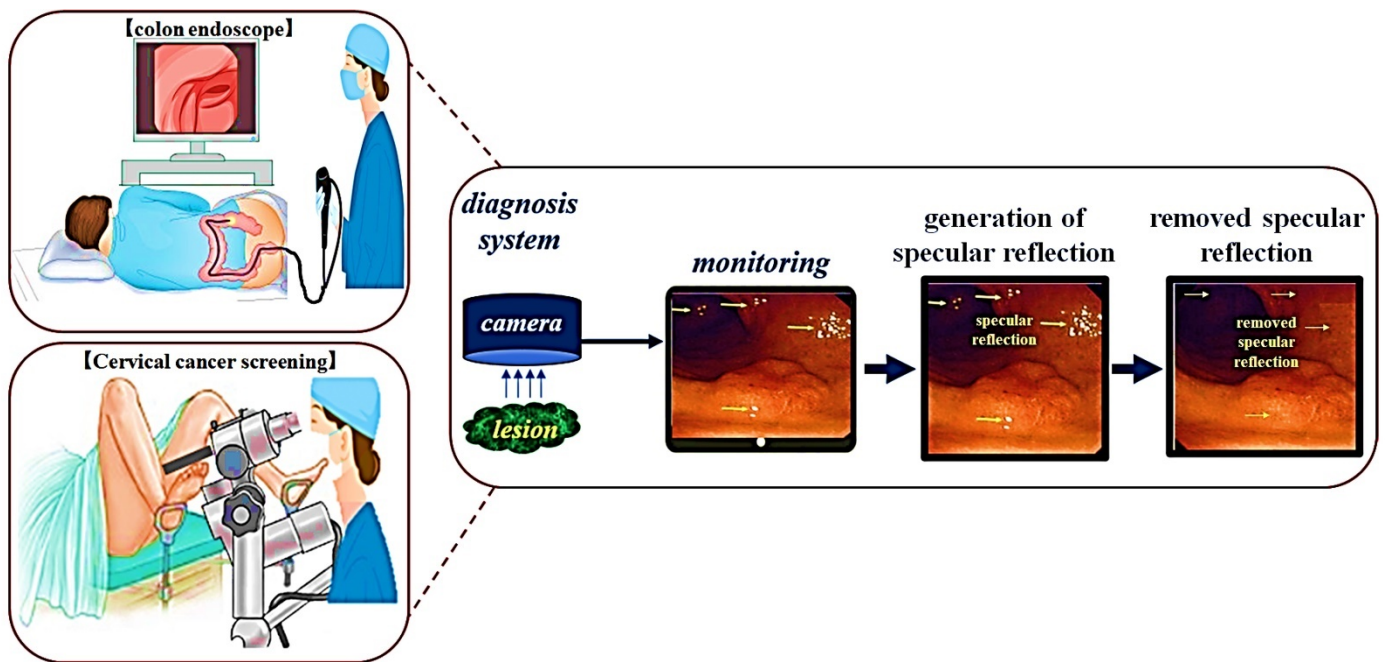


Figure 1. Generation of specular reflection in the diagnosis progress (The occurrence of light reflections from colonoscopy diagnosis and cervical endoscopy. In addition, the phenomenon of obstructing the observation of the lesion due to the occurrence of light reflection).

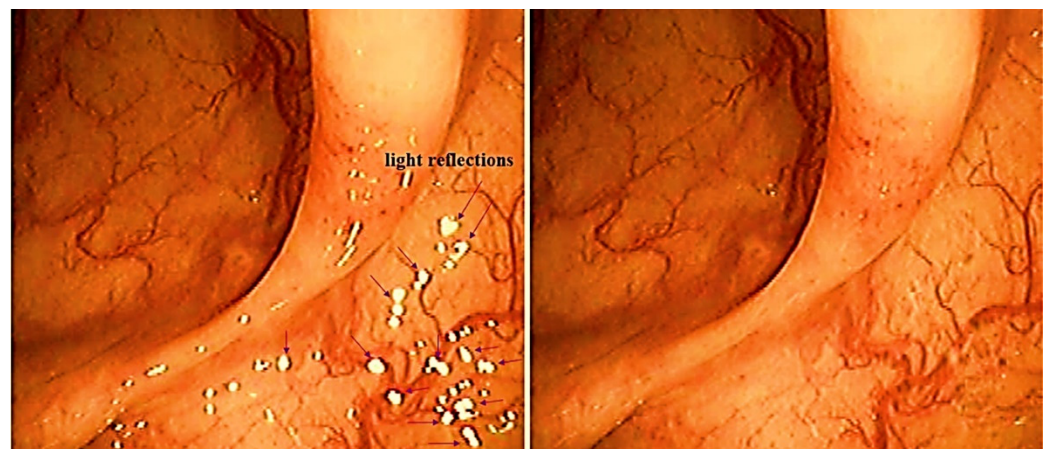


Figure 2. Creation of specular reflection through the LED with colon endoscopy and specular reflection removal.

To remove light reflection, two filters (E_1 , E_2) are configured, as shown in Figure 3. In Figure 3, E_1 and E_2 are the first and second polarization filters, and the E and H are the electric and magnetic fields of polarization. LPL is linear polarization. p_1 , p_2 , and p_3 are the positions where the image and light pass through the filter, and E_s is the sum of E_z and H_z ($E_s = E_z H_z$). In this case, E_z is vertical polarization and H_z is related to horizontal polarization. Consequently, the image and light are mixed together. E_o is a mixture of image and light with the same horizontal polarization as E and H . E_p means an image from which the $E_{x,y}$ component (light reflection) is removed and the light reflection in which only the H_y component remains.

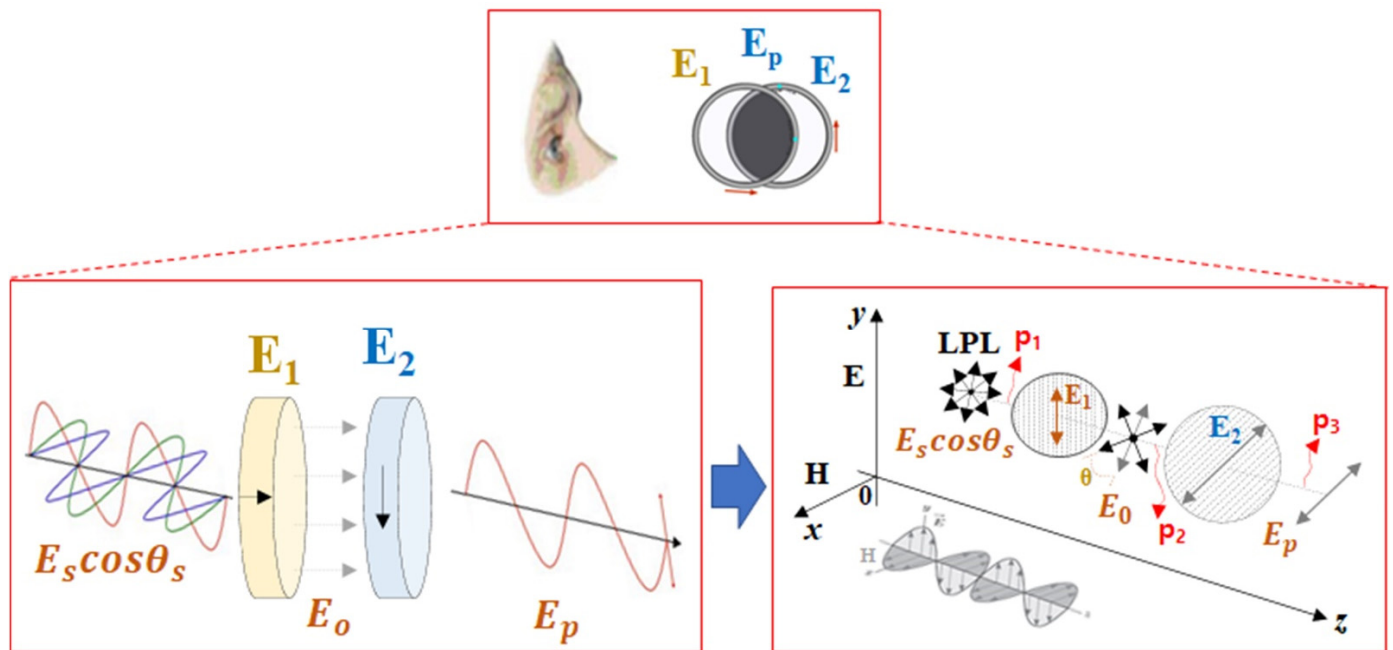


Figure 3. Analysis of specular removal through the linear polarized filtering.

In the figure, the light ($E_s \cos \theta_s$) of p_1 incident on the camera through the imaging of the lesion has vertical polarization (E_y) and horizontal polarization (E_z) proceeding in the x , y , and z directions as shown in Equations (1) and (3) ($E_y = 1, H_x = 1$) is assumed [20,21]. In the formula, $E_{z(y,x)}$ means E_z of magnitude in the y and x directions. θ denotes the filter rotation direction angles of E_1 and E_2 . In the z -direction light (p_2) passing through the polarization filter of E_1 , E_o , and E_s are changed to horizontal polarization ($E_y = 0, H_x = 0$), which is the sum of E_o and E_s , resulting in $E_o = E_s = 0$ [20,21].

$$E_z = E_y \cos \omega \theta_t \tag{1}$$

$$H_z = H_x \cos \omega \theta_t \tag{2}$$

$$\sum E_z = E_y + E_x = \begin{cases} E_z = E_{z(y)} e^{j(kz - \omega t + \theta)} \\ E_y = E_{z(x)} e^{j(kz - \omega t + \theta)} \end{cases} \tag{3}$$

The z -direction light (p_3) passing through the filter of E_2 only passes through E_o in the horizontally polarized state. Then, E_o becomes $E_o \neq E_s$, and E_o becomes $E_o = 0$. Since the phase of E_o may differ by 0 or an integer multiple of 2π , E_o proceeds in the x -direction as in Equations (4) and (5). All of the polarized waves of E_o moving in the x -direction are changed to horizontal polarization ($E_o = 0$), and the image is changed to a state in which light reflection is removed [21]. Finally, concerning E_o (p_2), as in Equation (6), vertical polarization and horizontal polarization differ by π in the z direction. Eventually, only the horizontal polarization corresponding to $\pi/2$ passes through the polarization filter of E_2 , resulting in reduced light reflection. An image (E_p of p_3) is provided [21].

$$E_o = E_y - H_y \cos \omega \theta_t \tag{4}$$

$$\sum E_o = E_{x(y)} e^{j(kz - \omega t + \theta_z)} + j E_y e^{j(kx - \omega t + \theta_y)} = [E_{x(y)} e^{j\theta_z} + j E_y e^{j\theta_y}] e^{j(kx - \omega t)} = E_{o(x,y)} e^{j(kx - \omega t)} \tag{5}$$

$$E_p = H_y \cos \omega \theta_t \tag{6}$$

where p_1 is polarized in the vector plane of x , y , and z , and has vertical and horizontal vibration directions (x, y) at a direction angle (θ) of 0° . The polarized waves p_1 of E_y and H_y passing through the first polarization filter E_1 oscillate p_2 in the vertical direction y . When

the direction angle θ of the second polarizing filter E_2 is 90° , only the E_y component passes through the vertical polarized wave of p_2 passing via the second polarizing filter E_2 , and the H_x intensity is weakened. The propagation angle of the polarization with respect to E_p can be analyzed using the ABCD matrix shown in Equation (7) and Figures 4 and 5 to reduce the light intensity according to the change in θ [21]. If the intensity of light $E_{(x,y)}$ with respect to polarization rotates from y to z and θ is $\cos 90^\circ$, light reflection is reduced to the zero (0).

$$E_p = \begin{bmatrix} E_x \\ E_y \end{bmatrix} = \begin{bmatrix} E_x e^{j(\theta_x)} \\ E_y e^{j(\theta_y)} \end{bmatrix} = \begin{bmatrix} a \\ b \end{bmatrix}, |a|^2 + |b|^2 = 1 \tag{7}$$

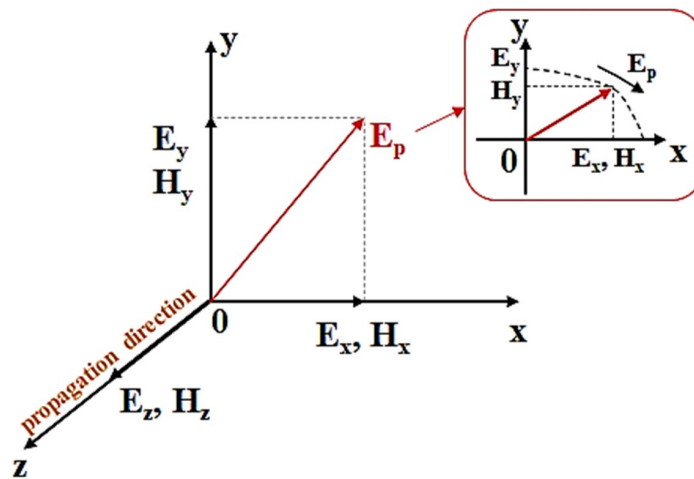


Figure 4. Direction of filter rotation angle (E_2).

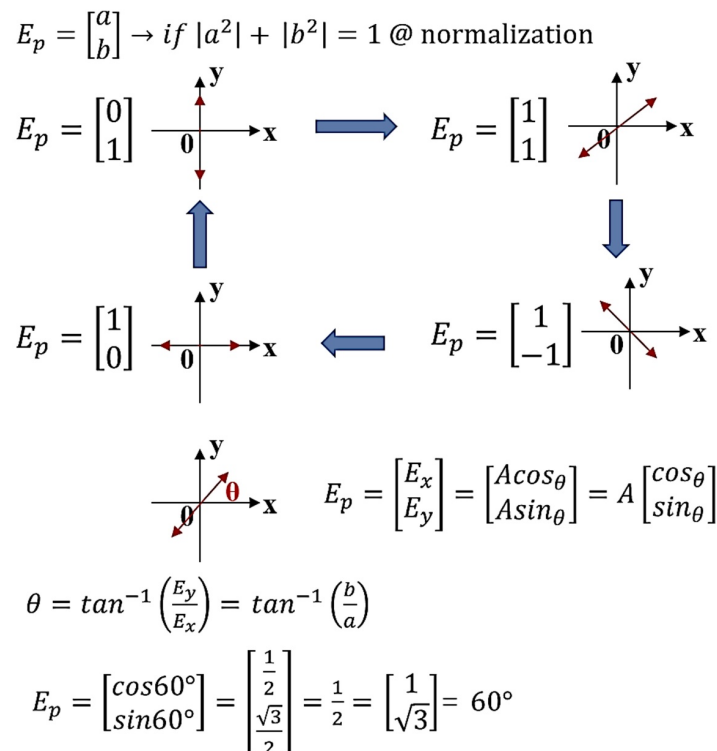


Figure 5. Polarization (specular reflection) propagation direction with respect to the rotation angle of the filter (E_2).

When θ becomes $\Delta\Phi_i$ ($\Delta\Phi_i |_{i = \phi_z - \phi_x} = 0, \pi/2, \pi/4, 3\pi/4, \pi$), the light intensity ($E_{o(x,y)}$) changes, as shown in Figure 6.

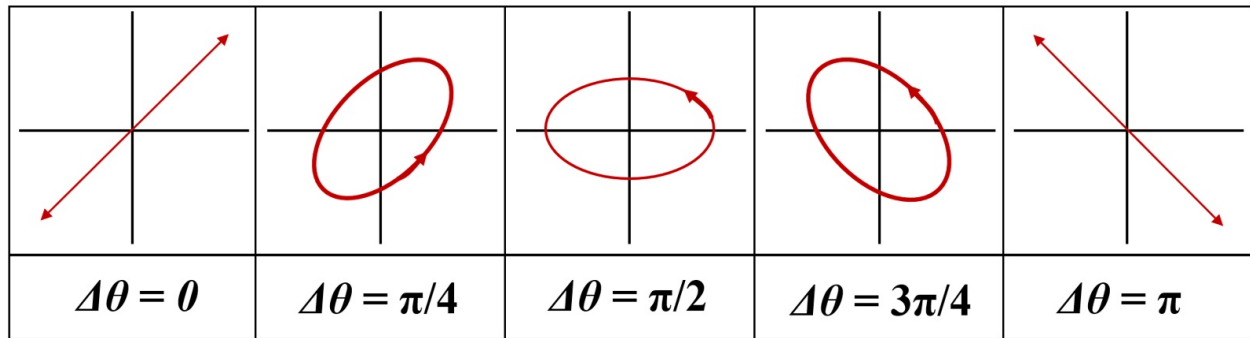


Figure 6. Characteristics of polarization according to the rotation angle of the filter (E_2).

For example, when the light reflection intensity (I_{ref}) passes through two filters ($\theta_{Ep} = 90^\circ$ difference) ($E_1 = 0^\circ, E_2 = 90^\circ$), the light reflection intensity (I_{ref}) at the p_3 position is reduced by more than half. Eventually, the intensity of light reflection (I_{ref}) is lowered by more than half compared to the intensity of light (I_{Ep}). The reason for this is that, as in Malus’s law in Equation (8), when the rotation angle of the first filter ($\theta_{ref} = 0^\circ$) is fixed, when the second filter is rotated at 90° ($\cos\theta_{Ep} = 90^\circ$), the intensity of light reflection (I_{ref}) becomes 0 [19–21].

$$I_{ref} = I_{Ep} \cos^2 \theta_{Ep} = \left(\frac{I_{Ep}}{2}\right) \cos^2 \theta_{Ep} = I_{ref} - I_{Ep} = I_{ref} - \left[\left(\frac{1}{3}\right) I_{Ep}\right] = \frac{3(I_{Ep} - I_{Ep})}{3} = \left(\frac{1}{3}\right) I_{Ep} \quad (8)$$

If the I_{Ep} is 0 mW/cm^2 , the rotation angle (θ_{ref}) of the E_1 filter is 0° , and the rotation angle (θ_{Ep}) of the E_2 filter is 90° , as in Equation (9), the light reflection intensity (I_{ref}) is interpreted again as 50 mW/cm^2 , as given in by Table 1, when I_{Ep} is 0 mW/cm^2 ($\theta_{Ep} = 90^\circ$). At this time, when the rotation angle θ_{ref} of the E_1 filter is 0° , the rotation angle θ_{Ep} of the E_2 filter corresponds to 0° to 360° .

Table 1. Analysis of changes in light reflection intensity according to the rotation angle of the filter ($E_2 @ E_1 = 50 \text{ mW/cm}^2$).

E_2 Rotation Angle of the Filter (θ_{Ep})	Light Reflection Intensity [mW/cm^2]	E_2 Rotation Angle of the Filter (θ_{Ep})	Light Reflection Intensity [mW/cm^2]
0°	50.0	210°	37.5
30°	37.5	240°	12.5
60°	12.5	270°	0.00
90°	0.00	300°	12.5
120°	12.5	330°	37.5
150°	37.5	360°	50.0
180°	50.0		

$$I_{ref} = I_{Ep} \cos^2 \theta_{Ep} = (50 \times 10^{-3}) \cos^2(0^\circ - 90^\circ) = (50 \times 10^{-3}) \cos^2(90^\circ) = (50 \times 10^{-3})(0)^2 = 0 \text{ mW/cm}^2 \quad (9)$$

When analyzing Equations (1)–(9) and Table 1, since the first polarizing filter (E_1) was fixed at 0° , the second polarizing filter (E_2) was sequentially rotated from 0° to 360° . Similarly, a phenomenon in which the intensity of light reflection decreases and rises is repeated like a sine wave. When the rotation angle θ_{Ep} of the E_2 filter is 90° or 270° , the intensity of light reflection becomes 0 mW/cm^2 , and a phenomenon in which light

reflection is removed arises. For this reason, as shown in Figure 7, when the rotation angle (θ_{Ep}) is 0° , light (light reflection) passes through the second polarization filter (E_2), and the light reflection intensity (I_{ref}) has a maximum value. That is, the intensities for I_{Ep} and I_{ref} are the same and they have an equilibrium relationship with each other. When the second polarizing filter E_2 rotates from 10° to 80° during the rotation process, I_{Ep} and I_{ref} are out of horizontal relationship.

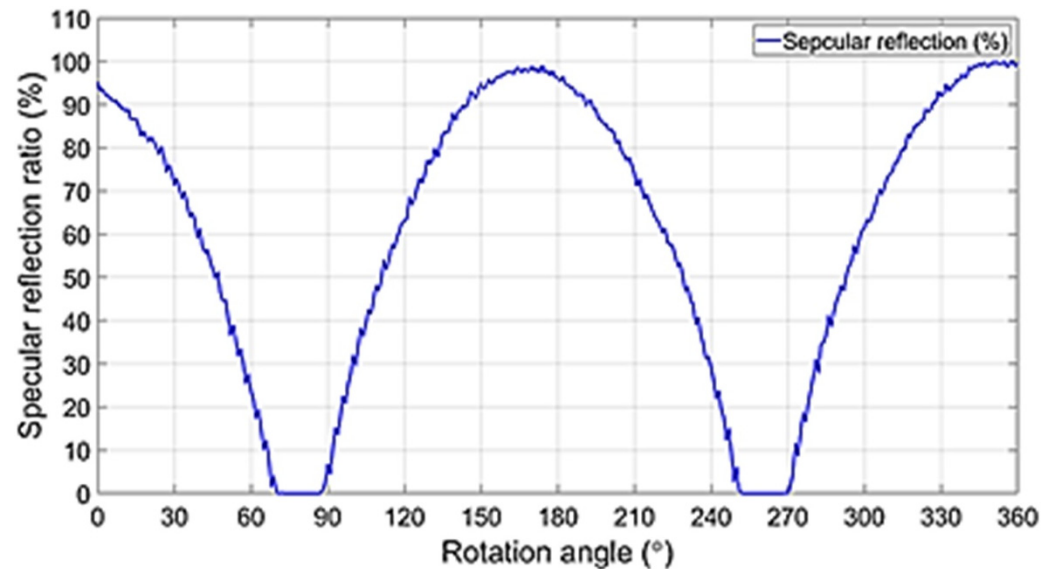


Figure 7. Changes in light reflection intensity according to the rotation axis of the filter using Malus's laws.

When the rotation axis of the second filter (E_2) reaches 90° , I_{Ep} and I_{ref} (the difference between $E_1 \neq E_2 = 90^\circ$ of the filter) intersect with each other, so that I_{Ep} has the maximum value ($I_{Ep} = 1$) and I_{ref} will have the minimum a value of ($I_{ref} = 0$). Consequently, the intensity of light reflection is lost, and the image quality is increased. If the rotation angle of the filter deviates from 90° ($<100^\circ$), I_{Ep} changes to the minimum value ($I_{Ep} = 0$) and I_{ref} changes to the maximum value ($I_{ref} = 1$). At this time, the I_{Ep} and I_{ref} will have the same value ($I_{Ep} = I_{ref}$). This phenomenon is repeated. To summarize, the method for maximally suppressing light reflection is that when the first filter E_1 is 0° , the second filter E_2 should be 90° . As a result, the polarized wave p_3 that has passed through E_2 outputs only the polarized wave E_p with reduced light reflection. As a result, the intensity of light loses its maximum value, and eventually, the intensity of light starts to decrease slowly, and when the rotation angle θ_{Ep} is 90° (270°), the intensity of light reflection (I_{ref}) becomes 0.

3. Experiment Composition and Results

In order to obtain the effect of reducing light reflection, the experimental device is configured as shown in Figure 8. The device for the experiment consists of a camera, an LPL filter, and an LED. The method followed to obtain the result uses phantom. The first polarizer filter connected in front of the camera has a rotation angle (θ) of 0° and the filter is fixed. However, the filter is in a polarization state. The second filter has a rotation angle (θ) of 0° and this filter is unpolarized. The filter connected to the LED changes the rotation angle (θ) from 0° to 360° , and the filter is rotated.

The filter for connection to the camera and LED was made using 3D printer technology to make a fixed frame, and the LED and filter are connected in this frame. The installation angle of the camera is 0° and the irradiation direction angle of the LED (the angle between the camera and the LED) is 30° . Moreover, the number of irradiated LEDs is 10. The working distance (WD) between the camera and the LED and the phantom is 14 cm.

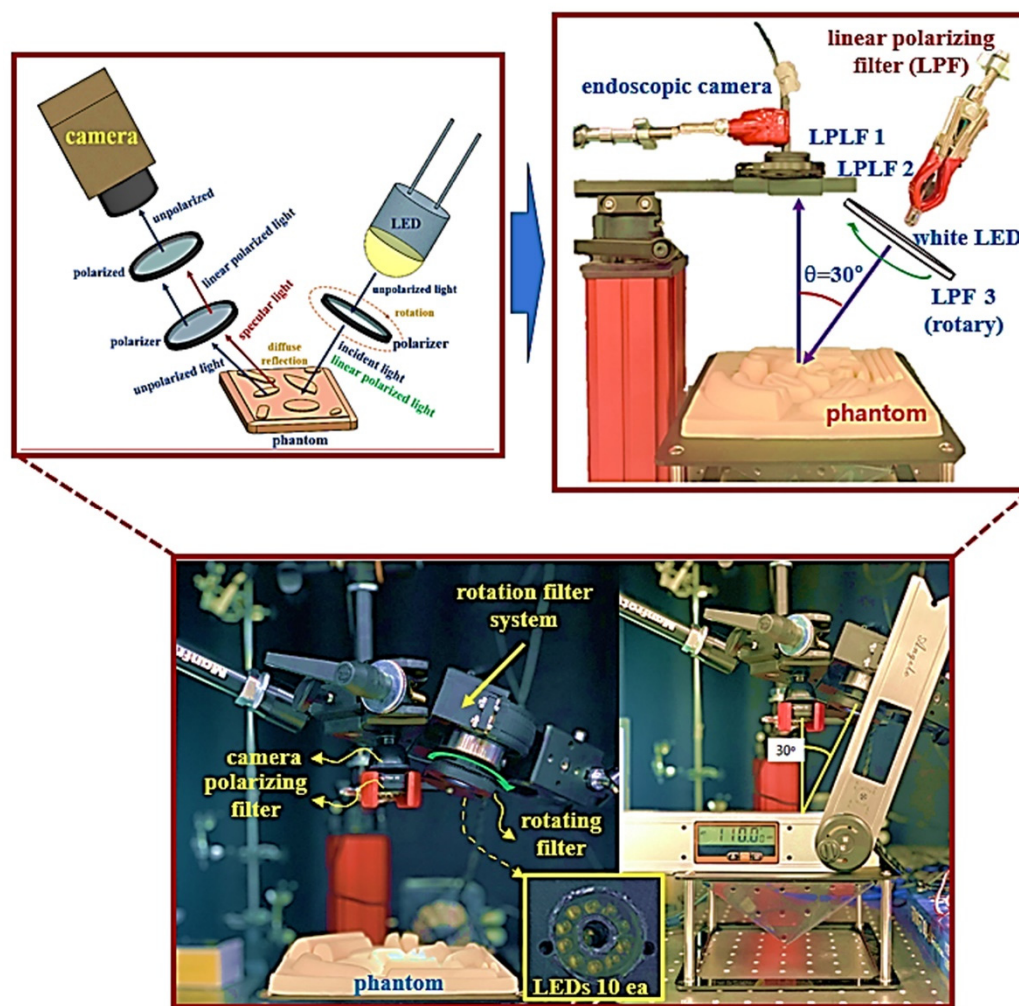


Figure 8. Experimental setup configuration.

The main parameters of the LED (010C3UC020, DAKWANG, Yantai, China), camera (Dr. Cervicam C20, NTL Healthcare, Seongnam, Republic of Korea), and filter used for the experiment are presented in Table 2.

Table 2. Experimental device module parameters.

Performance (@ LED)	Parameter	Performance (@ Camera)	Parameter
model	LED (010C3UC020)	model	SJ-8200
wavelength, λ [nm]	465–470	sensor	CMOS
output power [mW]	50	Resolution [P]	1920
current [mA]	20	pixel size [M_{pixel}]	2.0
voltage [V]	2.5	frame rete [fps]	30
beam angle of radiation, θ [deg]	40	focal distance	5 mm–infinity
luminous intensity [mrcd]	2500	view angle [deg]	60°

For the use of a linear polarized filter (Schneider-Kreuznach, Schneider (1.25 inch), 155543, Bad Kreuznach, Germany), the wavelength band is 420–750 nm and the diameter of the lens is 27 mm. In addition, the thickness of the filter lens is 0.25 mm, and the transmittance is 34%. Extinction ratio is >10.000:1 and the LPL filter is uncoated.

The experimental results using phantom are shown in Figure 9. From the figure, specific reflection is generated on the phantom. The arising position of the specific reflection is indicated by a yellow arrow. As a result of using the filter, when the rotation angle (θ) of the filter connected to the LED is 0° – 360° , it can be observed that light reflection is reduced, and the rotation angle (θ) is 90° . When it is analyzed, that light reflection is reduced.

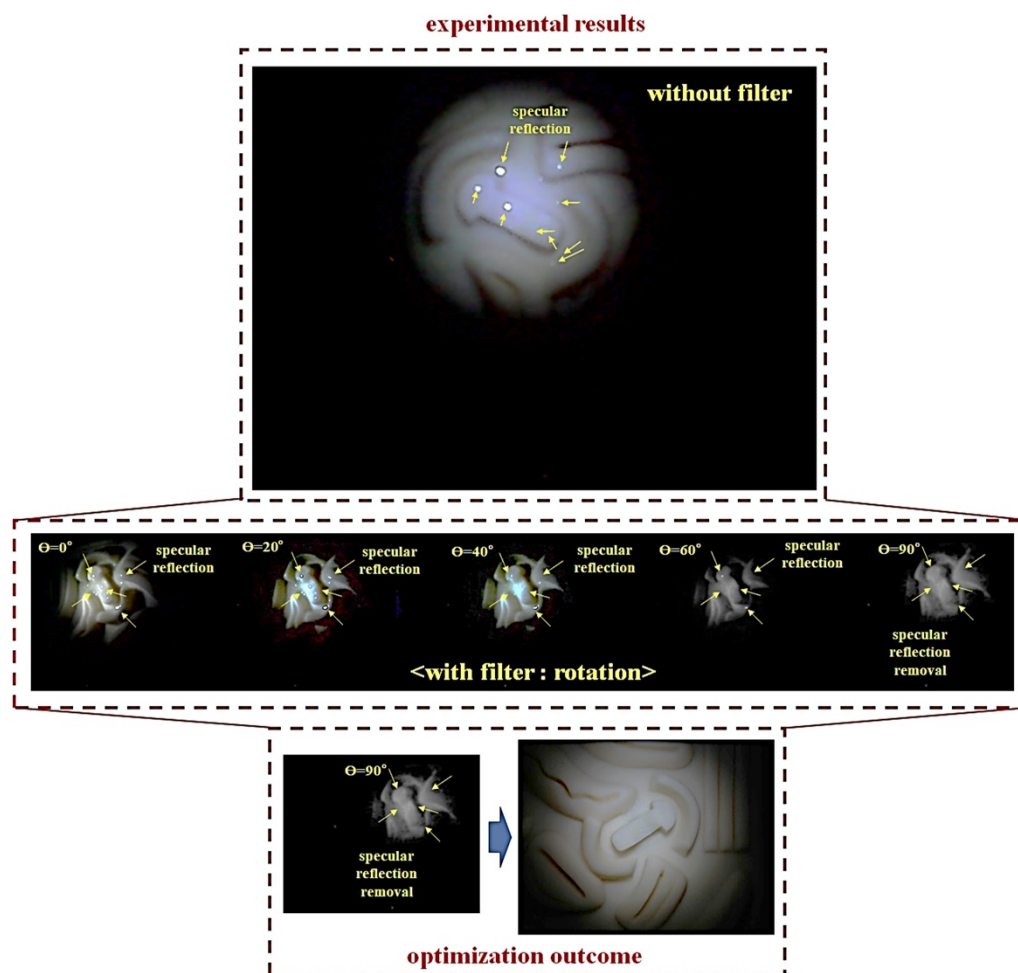


Figure 9. Phantom experiment result for removal specular reflection.

The captured image results were simulated using an ROI (region of interesting) program (PyCharm. JetBrains, Prague, Czech Republic), as shown in Figure 10. In the simulation result, when the rotation angle θ of the filter is 0° , the light reflection generation position is indicated by a yellow point. In this case, the intensity (intensity of light) corresponds to 0 in the area where light reflection does not occur in the histogram. However, since most of the light reflection is generated to the phantom, the light reflection intensity is no longer 0. Therefore, the intensity of light reflection has a value of 25–294, and the maximum intensity of light reflection is 294. However, when the rotation angle (θ) of the filter was 90° , the intensity of light reflection changed to 0.

Figure 11 shows the human tissue test results for the phantom imaging results in Figure 9 for the reliability performance test. For the reliability of the study, this experiment was conducted three times. In order to increase the reliability of the research methodology, direct pictures were taken using my own oral cavity instead of a phantom. In the experimental results, light reflection happens when the LPL filter was not applied, but when the rotation angle (θ) of the filter is adjusted from 0° to 360° using the LPL filter, when the rotation angle was 90° , the light reflection was sufficient and could be removed.

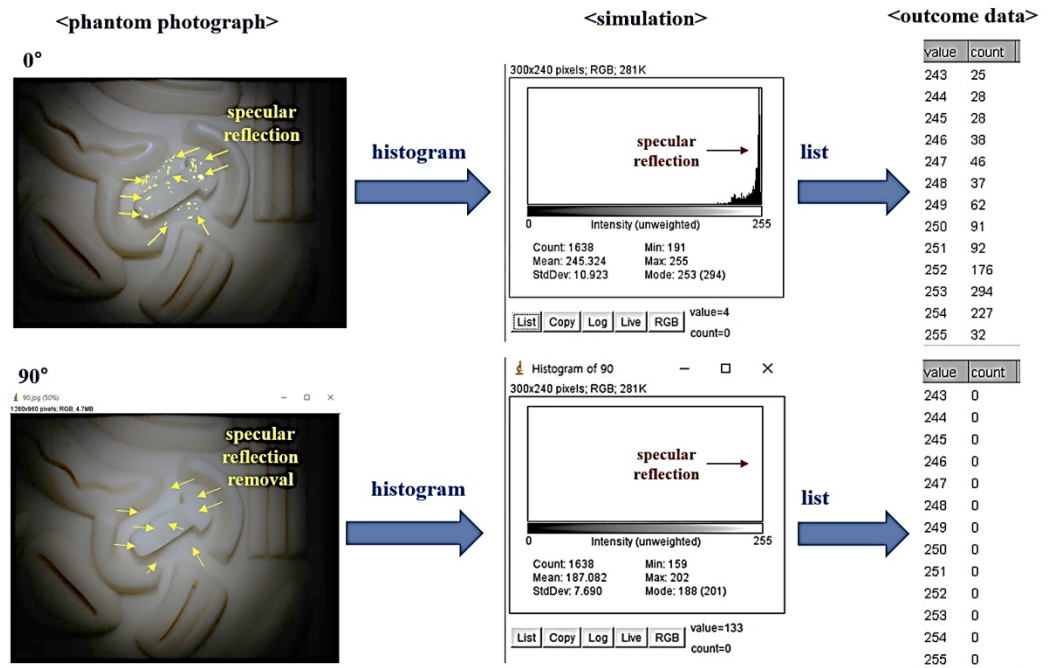


Figure 10. ROI Numerical analysis of Phantom experiment results for specular reflection removal.

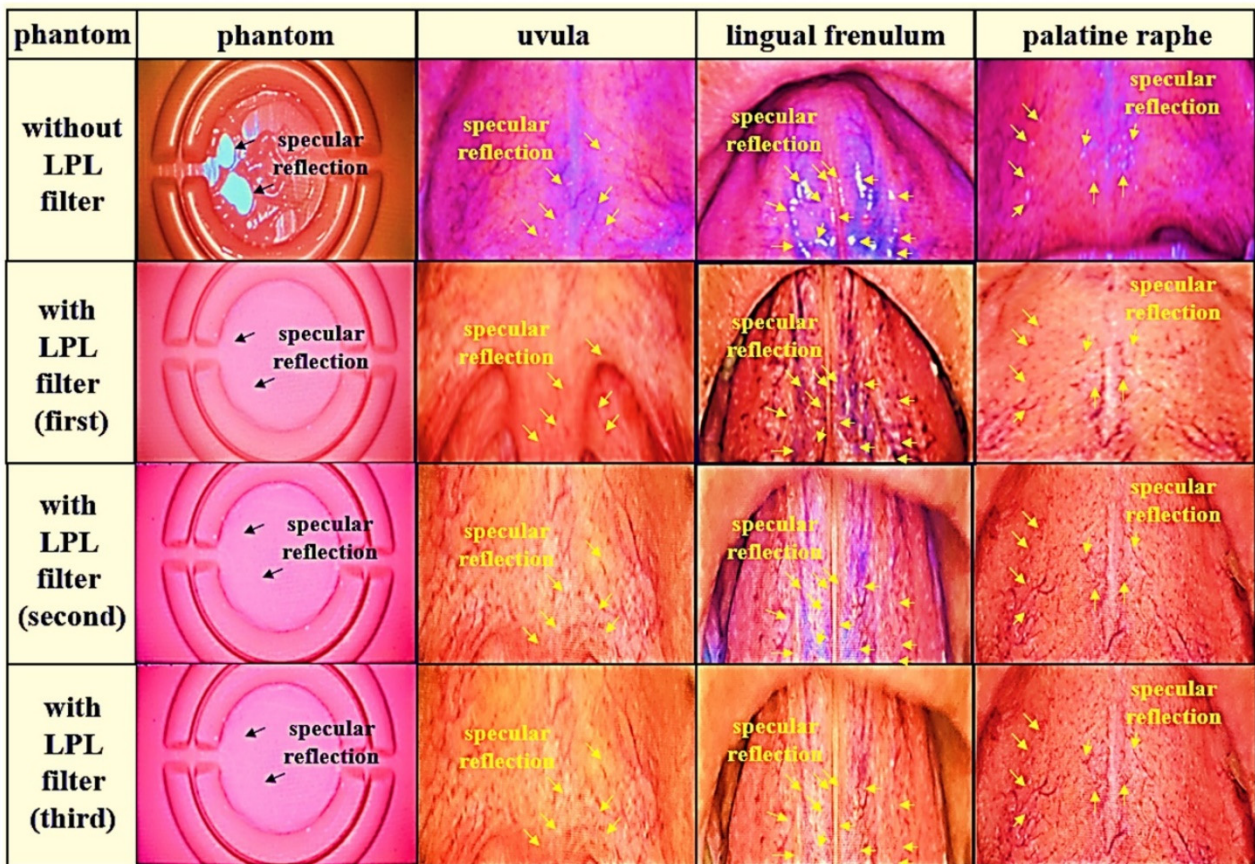


Figure 11. Experimental results of removal specular reflection through oral imaging.

In Figure 11, when the LPL filter was used, the phantom, uvula, lingual frenulum, and palatine raphe had light reflections like yellow markers. When the LPL filter (first) is used, the phantom, uvula, lingual frenulum, and palatine raphe, like yellow markers, have

light reflections removed so that the image looks clear. When the reproduction test (second and third) was performed to obtain a reliable image to obtain the effect of removing light reflection when the LPL filter is used, the image result of the first LPL filter was similar.

4. Discussion

This study proposes a method to efficiently reduce the light reflection of images generated by diagnostic systems, such as microscopes, endoscopes, and cameras.

The mention of the genesis of light reflexes in all tissues is cautious. However, soft fibrous tissues, such as the stomach, colon, and cervix, for endoscopic diagnosis are confirmed in the clinical field as light reflection generates. When the LED is irradiated to the tissue mucosa, light reflection rises according to Snell's law. Ambient reflection, diffusive reflection, and specular reflection are highly likely to occur because of the difference between the density of the cavity, the tissue density, and the moisture density of the tissue as the cause of light reflection [22].

In the light of the LED irradiated from the cavity, both the absorbed light and the reflected light are generated at the same time because of the density at the water surface interface or the tissue surface interface. The reflected light causes scattering, which prevents monitoring through camera shooting.

In the experimental process, the light reflection intensity is almost identical in the wavelength band of 400–1100 nm. Vertical polarization and horizontal polarization are generated together in the wavelength range. For that reason, it is important to eliminate all vertical polarizations. The wavelength band of 400–1100 nm is a white light source LED. During the endoscopic procedure, white light (LED) is used to brightly image the dark tissue space. Light reflections are severe in white illuminated LEDs (400–1100 nm). In order to reduce light reflection, it is inconvenient to adjust the orientation angle of the camera or adjust the brightness of the LED at the clinical diagnosis site [9]. However, using these methods, it is not easy to obtain clear diagnostic results in the clinical diagnosis process. In particular, if the camera orientation angle is adjusted, the lesion shape observation angle may be changed. In addition, if the brightness of the LED is adjusted, it is observed with a dark background. Accordingly, it is time-consuming and cumbersome to correct the photographing result using an imaging process. For quick and accurate diagnosis, a clear image must be provided, and light reflection must be removed to secure the observation field of the lesion. Accordingly, it is judged that the evaluation of the method of removing light reflection of the camera will contribute a lot to the clinical diagnosis phenomenon.

In this study, a phantom (a silicone material for suturing practice) was used instead of an animal experiment to examine the effect of light reflection removal, and the tissue in Figure 11 was taken using my oral cavity. Consequently, the experiment through oral imaging was repeated three times and the reliability of the results was increased. If a filter made of film material is used, it is judged that the proposed method can be sufficiently commercialized by applying it to a camera shooting system. Thereby, if excellent results are obtained through clinical trials, it is expected that the use value in the field of clinical diagnosis will increase.

5. Conclusions

This study proposes a method for removing light reflection in diagnostic imaging systems, such as microscopes, endoscopes, and cameras, and proves the possible results through experiments. The main method for the proposed study is to control the polarization using the rotation angle of the filter. Thus, by controlling the propagation directions of the vertical and horizontal polarizations, the light reflection for the vertical polarization is removed and only the horizontal polarization for the video image can pass through. A phantom was used to obtain the experimental results, and the photographic experiments were repeated three times through the oral tissue to prove the high reliability of results. In consequence, the oral imaging results were consistent with the phantom test results without any light reflection.

When an LPL filter was used, light reflection is generated to the phantom and tissue. However, when the LPL filter (first) was used, the image showed the light reflection removed from the phantom and tissue. Moreover, a reproduction test was conducted to obtain a reliable image, and the image result was similar to the image result of the first LPL filter.

The proposed method eliminates light reflection in real time at the diagnostic imaging site without additional imaging software correction processing, providing excellent imaging. Thus, it is possible to secure a field of view for observation of the lesion through clear imaging results and to obtain fast and accurate diagnosis results. In addition, the advantage of the proposed method can be connected to all cameras, microscopes, and endoscopes regardless of the size of the filter, so it can be applied to clinical diagnosis sites. So, the research method is highly practical. It is expected that this research method can be sufficiently applied to clinical diagnosis sites through product design and clinical trials in the future.

Author Contributions: Design and experiment, K.Y.; analysis and fabrication, J.S.; guidance and supervision, K.G.K. All authors have read and agreed to the published version of the manuscript.

Funding: This research was supported by the MSIT (Ministry of Science and ICT), Korea, under the ITRC (Information Technology Research Center) support program (IITP-2021-2017-0-01630) supervised by the IITP (Institute for Information & Communications Technology Promotion), and by the GRRC program of the Gyeonggi province (No. GRRC-Gachon2020(B01)), respectively. In addition, the research was supported by the G-ABC FRD2019-11-02(3).

Institutional Review Board Statement: Not applicable.

Informed Consent Statement: Not applicable.

Data Availability Statement: The data presented in this study are available upon request from the author.

Acknowledgments: Kicheol Yoon and Jaehwang Seol equally contributed to the work. Kicheol Yoon and Jaehwang Seol are the co-first (lead) authors.

Conflicts of Interest: The authors declare no conflict of interest.

References

1. Lee, S.H.; Kim, J.Y. Artificial intelligence technology trends based on medical big data. *J. Korean Inst. Commun. Sci.* **2020**, *37*, 85–91.
2. Park, C.H.; Yang, D.H.; Kim, J.W.; Kim, J.H.; Kim, J.H.; Min, Y.W.; Lee, S.H.; Bae, J.H.; Chung, H.; Choi, K.D.; et al. Clinical practice guideline for endoscopic resection of early gastrointestinal cancer. *Korean J. Gastroenterol.* **2020**, *53*, 142–166.
3. Lee, B.E.; Kim, G.H.; Park, D.Y.; Kim, D.H.; Jeon, T.Y.; Park, S.B.; You, H.S.; Ryu, D.Y.; Kim, D.U.; Song, G.A. Acetic acid-indigo carmine chromoendoscopy for delineating early gastric cancers: Its usefulness according to histological type. *BMC Gastroenterol.* **2010**, *23*, 97. [[CrossRef](#)] [[PubMed](#)]
4. Kato, M.; Kaise, M.; Yonezawa, J.; Toyozumi, H.; Yoshimura, T.; Yoshida, Y.; Kawamura, M.; Tajiri, H. Magnifying endoscopy with narrow-band imaging achieves superior accuracy in the differential diagnosis of superficial gastric lesions identified with white-light endoscopy: A prospective study. *Gastrointest. Endosc.* **2010**, *72*, 523–529. [[CrossRef](#)] [[PubMed](#)]
5. U.S. Department of Health and Human Services. Guidance for Industry Standards for Clinical Trial Imaging Endpoints. Available online: <http://www.fda.gov/drugs/guidance-compliance-regulatory-information/guidances/default.htm.2011.08> (accessed on 11 January 2022).
6. Xie, X.; Li, G.; Chi, B.; Yu, X.; Zhang, C.; Wang, Z. Micro-system design for wireless endoscopy system. In Proceedings of the 2005 IEEE Engineering in Medicine and Biology 27th Annual Conference, Shanghai, China, 1–4 September 2005; pp. 1–4.
7. Feldman, M.K.; Katyal, S.; Blackwood, M.S. US artifacts. *Radiographics* **2009**, *29*, 1179–1189. [[CrossRef](#)] [[PubMed](#)]
8. Jiao, J.; Fan, W.; Sun, J.; Satoshi, N. Highlight removal for camera captured documents based on image stitching. In Proceedings of the International Conference on Signal Processing, Washington, DC, USA, 6–10 November 2016.
9. Meleppat, K.R.; Zhang, P.; Ju, M.J.; Mamma, S.K.; Jian, Y.; Pugh, E.N.; Zawadzki, R.J. Directional optical coherence tomography reveals melanin concentration-dependent scattering properties of retinal pigment epithelium. *J. Biomed. Opt.* **2019**, *24*, 066011. [[CrossRef](#)] [[PubMed](#)]
10. Wan, R.; Shi, B.; Duan, L.Y.; Tan, A.H.; Kot, A.C. Benchmarking single image reflection removal algorithm. In Proceedings of the International Conference on Computer Vision, Venice, Italy, 29 October 2017.
11. Li, C.; Yang, Y.; He, K.; Lin, S.; Hopcroft, J.E. Single image reflection removal through cascaded refinement. *Comput. Vis. Pattern Recognit.* **2019**, 3565–3574.

12. Tchoulack, S.; Pierre Langlois, J.M.; Cheriet, F. A video stream processor for real-time detection and correction of specular reflections in endoscopic images. In Proceedings of the Circuits and Systems and TAISA Conference, Montreal, QC, Canada, 22–25 June 2008; pp. 49–52.
13. Wang, J.; Eng, H.; Kam, A.H.; Yau, W. Specular reflection removal for human detection under aquatic environment. In Proceedings of the Computer Society Conference on Computer Vision and Pattern Recognition Workshops, Washington, DC, USA, 27 June 2004.
14. Yamazaki, M.; Chen, Y.; Xu, G. Separating reflections from images using kernel independent component analysis. In Proceedings of the 18th International Conference on Pattern Recognition, Hong Kong, China, 20–24 August 2006; Volume 3, pp. 194–197.
15. Hodgson, A.; Kelly, N.; Peel, D. Unmanned aerial vehicles (UAVs) for surveying marine fauna: A dugong case study. *PLoS ONE* **2013**, *8*, e79556. [[CrossRef](#)]
16. Ahn, J.; Nishida, K.; Ishii, Y.; Ura, T. A sea creatures classification method using convolutional neural networks. In Proceedings of the IEEE 18th International Conference on Control, Automation and Systems (ICCAS), PyeongChang, Korea, 17–20 October 2018.
17. So, H.R.; Oh, S.J.; Jin, G.G. Modified geometric step-based box-counting method to estimate the complexity of korean peninsula coastlines. *J. Inst. Control.* **2019**, *25*, 30–36.
18. Goncalves, J.; Henriques, R. UAV photogrammetry for topographic monitoring of coastal areas. *ISPRS J. Photogramm. Remote Sens.* **2015**, *104*, 101–111. [[CrossRef](#)]
19. Monteiro, M.; Stari, C.; Cabeza, C.; Martí, A.C. The polarization of light and Malus' Law using smartphones. *Phys. Teach.* **2017**, *55*, 264. [[CrossRef](#)]
20. Rosi, T.; Onorato, P. Video analysis-based experiments regarding Malus law. *Phys. Educ.* **2020**, *55*, 045011. [[CrossRef](#)]
21. Woźniak, W.A.; Kurzynowski, P.; Zdunek, M. Malus law—Interferometric interpretation. *Opt. Appl.* **2013**, *XLIII*, 237–246.
22. Wright, R.S.; Sweet, M. *OpenGL Superbible: The Complete Guide to OpenGL Programming for Windows NT and Windows 98*; Waite Group Press: Corte Madera, CA, USA, 1996.